International Journal of Microwave and Wireless Technologies

cambridge.org/mrf

Effect of skin thickness on electromagnetic dosimetry analysis of a human body model up to 100 GHz

Fatih Kaburcuk

Sivas University of Science and Technology, Sivas, Turkey

Research Paper

Cite this article: Kaburcuk F (2024) Effect of skin thickness on electromagnetic dosimetry analysis of a human body model up to 100 GHz. *International Journal of Microwave and Wireless Technologies*, 1–8. https://doi.org/10.1017/S1759078724000977

Received: 29 February 2024
Revised: 6 September 2024
Accepted: 15 September 2024

Keywords:
biological effects of electromagnetic fields; electromagnetic dosimetry; FDTD method; millimeter wave

Email: fkaburcuk@sivas.edu.tr

Abstract

The accuracy of electromagnetic (EM) exposure assessments depends mainly on the resolution of a voxel human body model. The resolution of the conventional human body model is limited to a few millimeters. In the millimeter wave (mmWave) frequency range, EM waves are absorbed by the superficial tissues in the human body. Therefore, resolution and skin thickness of the human body model are important for accuracy of the EM wave exposure metrics recommended by international human safety guidelines. Realistic thickness modeling of the skin tissue on the human body may provide greater accuracy in the EM exposure assessment, especially at mmWave frequency range. In this paper, effects of the skin thickness on the EM exposure metrics in one-dimensional multi-layered models obtained from different regions of the body model are investigated using the dispersive algorithm based on the finite-difference time-domain method over the frequency range from 1 to 100 GHz. Furthermore, effects of eyelid tissue in a human eye on the EM exposure metrics are studied over the frequency range. The EM exposure metrics such as absorbed power density, heating factor, and power transmission coefficient are calculated up to 100 GHz to evaluate the limits of EM wave exposure.

Introduction

The rapid advancements of wireless and satellite communications technologies and radar technologies require radio-frequency electromagnetic (EM) waves radiated at higher operation frequencies to achieve higher data transfer rates and greater bandwidth. The EM waves radiated from devices operated at millimeter wave (mmWave) frequency range have raised many concerns about potential health risks to a human body. Numerous studies [1–4] have been conducted on the adverse health effect of EM radiation at mmWave frequency range. There are many health risks to humans that have not been scientifically proven, such as ocular effects [4], male fertility, glucose metabolism, skin burns, sleeping disorders, and EM hypersensitivity [4] due to exposure to non-ionizing radio-frequency EM waves. Additionally, some researchers [5, 6] investigate the relation between very long-term radio-frequency EM exposure generated by a cellular telephone and the risk factor of brain tumor formation.

To protect the human body from the adverse health effects of EM wave exposure, basic restrictions for EM wave exposure metrics such as specific absorption rate (SAR), incident power density (IPD), and absorbed power density (APD) are recommended for the public and occupational exposure scenarios over the frequency range from 100 kHz to 300 GHz by international human safety guidelines/standards which are International Commission on Non-Ionizing Radiation Protection (ICNIRP) [7] and IEEE International Committee on Electromagnetic Safety (IEEE-ICES) [8] revised in 2020 and 2019, respectively. The SAR averaged over 10-gram tissues (SAR_{10g}) is an appropriate measure for local temperature rise in tissues over the frequencies below 6 GHz. The SAR_{10g} is no longer a meaningful measure to evaluate EM exposure over the frequency range above 6 GHz. Therefore, these guidelines recommend the APD which is defined as a new EM exposure metric at frequency range between 6 GHz and 300 GHz and directly related to IPD over an area of 1 cm^2 and 4 cm^2. The IPD considered as a reference level in the ICNIRP guideline is defined as 10 W/m^2 and 50 W/m^2 at frequencies above 2 GHz for the public and occupational exposure scenarios, respectively. Furthermore, heating factor defined as a ratio of the temperature rise to APD is a useful metric for evaluating the thermal effect due to EM wave exposure at frequencies above 6 GHz. The ratio of total power deposition (TPD) and IPD gives the power transmission coefficient (PTC) [9], which is used to evaluate transmission from air to the skin tissue of the human body.

For EM dosimetry analysis of the human body, computational EM methods play an important role due to the lack of analytical solutions for the human body. In most EM

dosimetry studies, the finite-difference time-domain (FDTD) method has been used due to its suitability for complex, inhomogeneous, dispersive, and voxel-based structures such as a human body. The interaction between three-dimensional (3D) human body parts such as a head model and EM exposure sources [10–18] at frequencies below 6 GHz has been investigated using the FDTD method. Furthermore, one-dimensional (1D) multi-layered human body models due to EM waves radiated by the far-field sources have been investigated in [19–23] using the FDTD method. The EM waves propagating from EM sources penetrate deeply into biological tissues because the frequency-dependent penetration depth is approximately higher than 15 mm at frequencies below 6 GHz [22]. Above 6 GHz, most EM waves are absorbed by the superficial tissues of the human body, especially by the skin tissue. The effects of EM waves generated by near-field and far-field exposure sources on the 3D realistic human body parts such as head, eye, and forearm models have not been analyzed except for a few studies [24–29] due to the cell size constraint of the FDTD method at mmWave frequency range. In order to satisfy the Courant–Friedrichs–Lewy (CFL) condition [30] in the FDTD method, the cell size must be at least one-tenth of the minimum wavelength of the tissues. Due to the cell size constraint, the FDTD computational domain may contain more than hundreds of millions of cells, which require very long computation time and large computer memory and could be impossible to perform EM analysis of the human body, especially if ordinary computers are used. However, in the mmWave frequency range, the whole human body model is not essential for the EM dosimetry analysis because EM waves cannot penetrate deep tissues. Therefore, a 3D multi-layered cube model, instead of the whole human body model, has been analyzed due to a near-field exposure source [28–31] in the mmWave frequency range. The realistic 1D multi-layered human body models presented in [22] and a simple 1D four-layered model in [9–23] are analyzed using the FDTD method at mmWave frequency range. In [32], a simple four-layered model is analyzed to show the effect of thickness of tissue layers on the temperature rise using Monte Carlo simulation over the frequency range from 10 GHz to 1 THz. However, EM analysis of 1D multi-layered models obtained from different regions of the human body has not been extensively investigated using the FDTD method at mmWave frequency to show the effects of different multi-layered models on the EM wave exposure metrics.

At mmWave frequency range, effects of skin thickness for the simple 1D four-layered model on the EM wave exposure metrics have been studied in [9]. These metrics are significantly affected by the change of skin thickness. Therefore, it is important to consider the realistic thickness of the skin tissue on the human body because more realistic modeling of skin thickness on the human body provides higher accuracy for the EM dosimetry, especially in the mmWave frequency range. The realistic skin thickness values on the five different regions (forehead, eye, chest, forearm, and thigh) of the human body are presented in [33] for Korean adults and listed in Table 1. The human body model [34] used in this work is originally surrounded by a 2 mm thick skin tissue, whereas the skin thickness of different parts of the realistic human body is not the same. The effects of skin thickness in the different regions of the human model on the EM wave exposure metrics have not been extensively investigated. Furthermore, effects of an eyelid in case of open and closed eye on the EM wave exposure metrics due to EM exposure have been studied in [35] from 0.9 to 10 GHz and in [36] at 30 GHz. However, they have not been extensively investigated over the frequency range between 1 and 100 GHz.

Table 1. Skin thickness [33] of different regions in the realistic human body

Body regions	Realistic skin thickness (mm)
Forehead	0.90
Eyelid	0.57
Chest	1.39
Forearm	1.17
Thigh	1.16

To show the effect of skin thickness and tissue arrangement, realistic 1D multi-layered models obtained from five different regions (forehead, eye, chest, forearm, and thigh) having different skin thicknesses due to EM far-field exposure are analyzed using the dispersive algorithm based on the FDTD method in the frequency range from 1 to 100 GHz. These models with the realistic skin thickness listed in Table 1 are also analyzed to observe the effect of skin thickness on the EM dosimetry analysis. The skin thickness makes a difference in the heating factors of the models up to 100 GHz. The distribution of APD in the models is highly affected by the skin thickness and tissue arrangement of the models at the frequency range between 1 and 100 GHz, whereas the APD values on the skin surface are slightly affected by the skin thickness at higher frequencies. In addition, eye models with and without eyelids for a thickness of 2 mm and 0.57 mm are investigated over the frequency range up to 100 GHz.

Computation methods and models

FDTD method and dispersive algorithm

The FDTD method is one of the well-known numerical methods and has been widely used for EM dosimetry analysis of the human body due to its suitability to handle inhomogeneous tissues of the human body. For the numerical accuracy of the FDTD method, the CFL condition depending on the cell size of the computational domain must be satisfied. The cell size (Δ_i) must be at least one-tenth of the minimum wavelength of the tissues in the computational domain because the finer cell size provides solutions with better accuracy, especially at higher frequencies. Therefore, to ensure this condition and obtain accurate solutions over the frequency range up to 100 GHz, the cell size of the human body model is set to $\Delta_i = 0.0625$ mm in this study.

The total-field scattered-field (TF/SF) formulation [30] integrated into the dispersive FDTD algorithm is used to generate an incident plane wave on the TFSF boundary. The incident plane wave considered as a far-field source is a Gaussian waveform including the frequency range up to 100 GHz. To terminate the FDTD computational domain, the convolution perfect matched layer boundary [30] condition is used in a dispersive algorithm proposed in [17, 18]. The dispersive algorithm consists of three sub-calculations. In the first sub-calculation, EM analysis of the human body model with dispersive tissues is performed using the Debye models integrated into the FDTD method with the auxiliary differential equation to obtain solutions up to 100 GHz in a single simulation. Secondly, SAR, APD, and PTC recommended metrics by the ICNIRP guideline to evaluate EM wave exposure in the tissues are calculated at over the mmWave frequency range up to 100 GHz. Finally, calculation of the temperature rise due to the EM wave exposure is performed for all frequencies of interest.

https://doi.org/10.1017/S1759078724000977 Published online by Cambridge University Press

Table 2. Three-term Debye parameters of human tissues from 20 GHz to 100 GHz [37]

Tissue	ε_∞	ε_{s1}	ε_{s2}	ε_{s3}	τ_1 $[e^{-9}]$	$\tau_2[e^{-9}]$	τ_3 $[e^{-9}]$
Skin	4.368	2.711	22.538	17.662	0.002	0.006	0.019
Fat	2.566	0.339	1.182	1.424	0.001	0.005	0.017
Muscle	4.490	3.793	29.742	19.355	0.002	0.006	0.017
Bone cortical	2.647	0.695	2.683	6.163	0.001	0.006	0.019
Bone marrow	2.565	0.335	1.158	1.407	0.001	0.005	0.016
Blood	4.498	3.684	32.111	26.674	0.002	0.006	0.021
White matter	4.315	2.212	18.093	14.502	0.002	0.006	0.018
Gray matter	4.428	3.123	25.887	20.335	0.002	0.006	0.019
CSF	4.614	4.717	39.895	31.694	0.002	0.006	0.024
Cerebellum	4.403	2.954	24.443	20.383	0.002	0.006	0.023
Lung	4.418	3.061	25.394	19.870	0.002	0.006	0.018
Heart	4.499	3.591	29.594	23.813	0.002	0.006	0.020
Kidney	4.491	3.497	28.628	24.139	0.002	0.006	0.022
Liver	4.345	2.401	20.938	20.001	0.002	0.006	0.019
Lens	4.376	2.803	23.427	18.053	0.002	0.006	0.017
Eye sclera	4.460	3.447	28.933	22.031	0.002	0.006	0.019
Cornea	4.465	3.452	28.828	22.807	0.002	0.006	0.022
Retina	4.460	3.447	28.933	22.031	0.002	0.006	0.019

The three-term Debye parameters (ε_∞: relative permittivity at infinite frequency, ε_{sk}: static relative permittivity, and τ_k: relaxation time at kth term) of 54 different tissues in the human body are based on the values presented in [37] and provide EM solutions at frequencies up to 100 GHz. These parameters of selected tissues from 20 GHz to 100 GHz are tabulated in Table 2. The complex relative permittivity $\left(\varepsilon_r^*(\omega)\right)$ in equation (1.a) and conductivity $(\sigma(\omega))$ in equation (1.b) for tissues is obtained from these parameters.

$$\varepsilon_r^*(\omega) = \varepsilon_r'(\omega) + j\varepsilon_r''(\omega) = \varepsilon_\infty + \sum_{k=1}^{3} \frac{\varepsilon_{sk} - \varepsilon_\infty}{1 + j\omega\tau_k} \tag{1.a}$$

$$\sigma(\omega) = -\varepsilon_r''(\omega) * \omega * \varepsilon_o \tag{1.b}$$

where ε_o is the permittivity of free space.

Human body model and 1D multi-layered models

A 3D realistic human body voxel model, named TARO in [34] and shown in Fig. 1(a), is used in this study and consists of 51 different tissues such as skin, fat, muscle, bone cortical and marrow, blood, white and gray matter, CSF, cerebellum, lung, heart, kidney, liver, eye tissues, etc. with a resolution of $\Delta_i = 2$ mm. The height and weight of the human body model used are 173 cm and 65 kg, respectively.

To satisfy the CFL conditions, the human body model with $\Delta_i = 2$ mm is resampled with all tissues to achieve a new human body model with $\Delta_i = 0.0625$ mm. 1D multi-layered models are then extracted from different regions of the human body model, including forehead, chest, forearm, thigh, and eye tissues with a high resolution. Therefore, effects of tissue arrangements of the models on the EM wave exposure metrics can be investigated. These 1D models presented in Fig. 1(b) and named forehead, eye, chest, forearm, and thigh models are marked as dashed lines on two-dimensional (2D) cross-sectional views of five different regions in the human body. The skin thickness and tissue arrangement of each model in the human body are different. Therefore, the forehead, chest, forearm, thigh, and eyelid models with different tissues arrangement, thickness of tissues and skin thickness are analyzed to have a more accurate assessment of EM dosimetry up to 100 GHz.

EM wave exposure metrics calculation

The SAR defined in [7, 8] is calculated to determine how much EM power absorbed per unit mass of tissues.

$$SAR_i = \frac{\sigma_i}{2\rho_i}|E_i|^2 \tag{2}$$

where $|E_i|$ [V/m], σ_i [S/m], and ρ_i [kg/m^3] are the total electric field strength, the electric conductivity, and mass density of the ith indexed cell of the tissues, respectively. The APD [29, 32, 38, 39] crossing a unit area at ith indexed cell is calculated as follows:

$$\mathrm{APD}_i = \frac{1}{2} Real\left[E_i \times H_i^*\right] \tag{3}$$

where E_i and H_i^* are the electric field and the complex conjugate of the magnetic field at ith indexed cell, respectively. For the assessment of the transmittance from air to skin tissue, the PTC [9] is the ratio of TPD and IPD. The TPD is calculated in equation (4) for the 1D multi-layered model.

https://doi.org/10.1017/S1759078724000977 Published online by Cambridge University Press

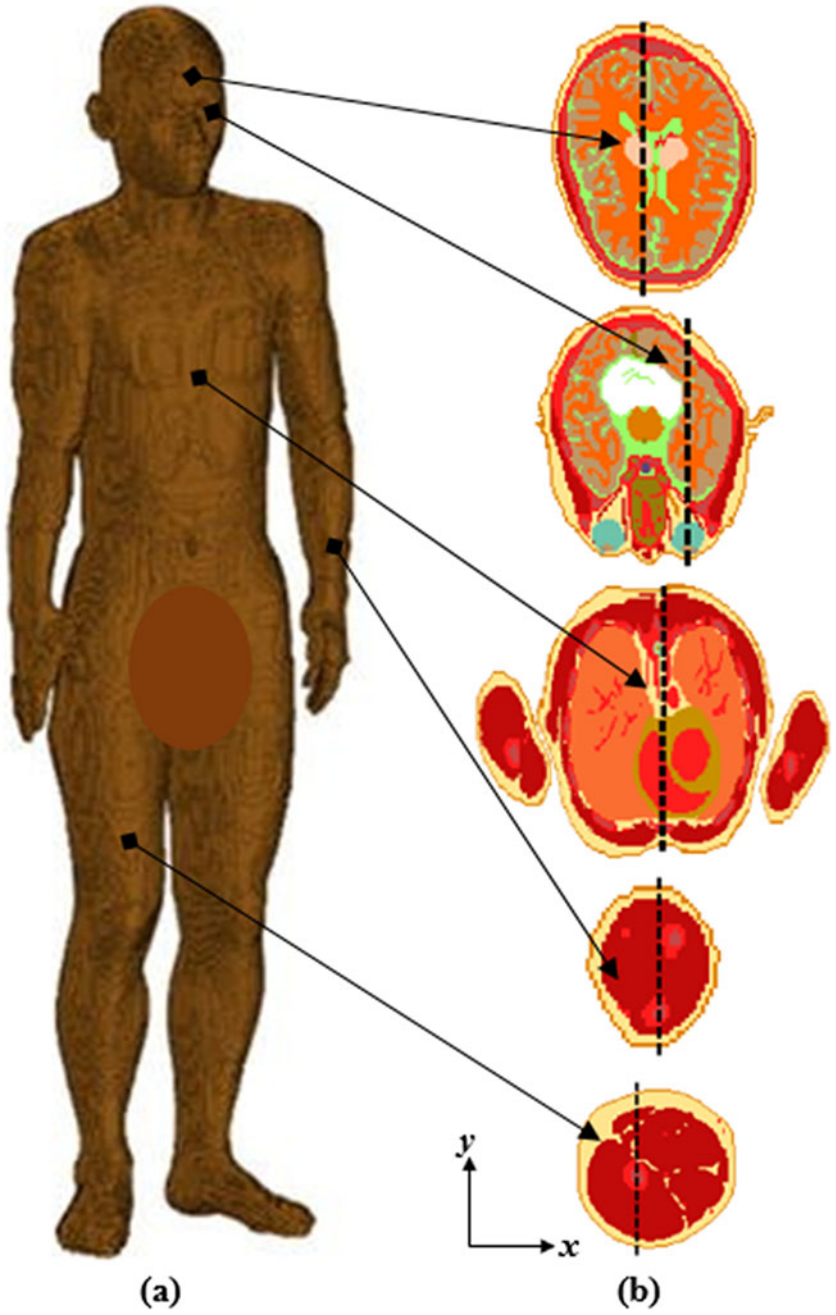

Figure 1. (a) 3D human body model [34], (b) 1D multi-layered models shown as dashed lines and derived from 2D cross sectional views (from top to bottom: forehead, eye, chest, forearm, and thigh models).

$$\mathrm{TPD} = \frac{1}{2}\int_{i=0}^{i_{max}} \sigma_i |E_i|^2 \mathrm{d}i \tag{4}$$

where i_{max} is larger than penetration depth.

Thermal calculation

The resting state temperature distribution in the human body model is calculated based on the Pennes bioheat equation [39] in the absence of a heating source (SAR = 0). The SAR distribution is considered as the heating source in the bioheat equation. Then, the final temperature rise distribution is computed by solving the bioheat equation again in the presence of the heating source (SAR ≠ 0). Finally, the temperature rise distribution is obtained by taking difference of the resting state and final temperature distributions.

The Pennes bioheat equation [40] is solved with the finite-difference approximation [21] at ith indexed cell of 1D multi-layered models with a resolution of Δ_i as follows:

$$T_i^{n+1} = T_i^n + \frac{\Delta_{temp,i}}{C_i} \times \left[SAR_i - \frac{B_i}{\rho_i}\left[T_i^n - T_b\right] + \frac{K_i}{\rho_i \cdot {\Delta_i}^2}\left[T_{i+1}^n + T_{i-1}^n - 2T_i^n\right] \right] \tag{5}$$

https://doi.org/10.1017/S1759078724000977 Published online by Cambridge University Press

where C_i [J/(kg·°C)], [W/(m·°C)], and B_i [W/(m^3·°C)] are the heat capacity, the thermal conductivity, and the blood perfusion rate at ith indexed cell of 1D multi-layered models, respectively. T_i^n is the temperature [°C] at time n and at ith indexed cell, and T_b is the blood temperature [°C] set to 37°C. The thermal time increment (Δ_{temp}) [10], used in the iterative calculation of the temperature in equation (5), must satisfy the numerical stability.

$$\Delta_{temp,i} \leq \frac{2 \cdot \rho_i \cdot C_i \cdot \Delta_i}{12 \cdot K_i + B_i \cdot \Delta_i^2} \tag{6}$$

At the interfaces of skin-air and internal cavity-air, the convective boundary condition is solved by the finite-difference approximation to model the heat exchange at the interfaces of skin-air and internal cavity-air. The convective boundary condition [10] is defined as

$$T_{i_{min}}^{n+1} = \frac{K_i \cdot T_{i_{min}+1}^n + T_{air} \cdot H \cdot \Delta_i}{K_i + H \cdot \Delta_i} \tag{7}$$

where T_{air} is the air temperature set to 20°C, n is the unit normal vector to the interfaces, and H is the convection heat transfer coefficient of 10.5 [W/(m^2·°C)] from the skin to air [10]. The mass density and thermal parameters of the human body tissues are based on the values presented in [41].

The heating factor based on the APD, which is defined as a ratio of the temperature rise to APD, is calculated as a function of frequency up to 100 GHz. Above 6 GHz, the maximum heating factor should be at most 0.025 [°C·m^2/W] based on [32].

Numerical results

The human body tissues in the 1D multi-layered models analyzed in this study are laid in the y-direction in which the incident plane wave propagates. The polarization of the incident plane wave is in the z-direction. The IPD of the incident plane wave is assumed as 10 W/m^2 at above 2 GHz. To verify the accuracy of the dispersive algorithm, the local SAR, SAR_{1g}, and SAR_{10g} values of the 1D multi-layered forehead model analyzed in this study are tabulated in Table 3 and compared with those values published in [22–25]. In [25], a thermal measurement has been made on the skin of a human forearm due to EM wave exposure for the IPD of 100 W/m^2, and then the temperature rise was found to be around 0.7°C at 77 GHz. In this study, the temperature rise in the 1D forearm model presented in Fig. 1(b) is 0.75°C at 77 GHz. Furthermore, a 3D voxel male head model with the resolution 0.5 mm has been analyzed numerically in [26] due to EM wave exposure for the IPD of 100 W/m^2 from 1 GHz to 10 GHz. At 10 GHz, the maximum SAR_{10g} and resulting temperature rise on the eye of the 3D head model are presented as 4.8 W/kg and 0.85°C in [26], respectively. For the comparison, the maximum SAR_{10g} and temperature rise in the 1D eye model without eyelid presented in Fig. 1(b) are found to be 4.28 W/kg and 0.84°C, respectively. The obtained results in this study are in good agreement with published results in [22] and [25, 26].

EM analysis of 1D multi-layered models

The realistic 1D multi-layered models consisting of forehead, eye, chest, forearm, and thigh tissues with 2 mm skin thickness shown in Fig. 1(b) are analyzed using the dispersive algorithm for the frequency range from 1 GHz to 100 GHz. Therefore, effects of five different 1D models on the EM exposure metrics are investigated due to the EM far-field public exposure based on the ICNIRP guideline.

For the sake of comparison, the APDs of the 1D multi-layered models with 2 mm skin thickness presented in Fig. 1(b) and a simple four-layered 1D forearm model with 1 mm skin thickness presented in [32] are shown in Fig. 2 as a function of tissue depth at 30 GHz for the IPD of 1000 W/m^2. It can be noticed from Fig. 2 that APDs of the forearm models presented in Fig. 1(b) and a forearm model presented in [32] are in good agreement inside the first 1 mm thickness of the skin. Then, the thickness of the skin and other tissues makes a difference on the APDs of the forearm models. After 2 mm skin tissue depth, the APD of the closed-eye model decreases faster than the APDs of other models because tissues in the eye models are different from the tissues in other models, and the APDs of other models decreases at different rates toward deeper tissues because the arrangement and thickness of tissues in all models are different.

The heating factors of the 1D forehead, chest, and forearm models are calculated up to 100 GHz for the IPD of 10 W/m^2. In Fig. 3, the obtained heating factors of the 1D models are compared with those presented in [23] of a simple 1D planar model. They have good consistency. Above 6 GHz, the maximum heating factors of all 1D models in the skin are less than 0.025 [°C·m^2/W], which is the maximum value of the heating factors recommended in [32]. Also, the heating factors of all models are in good consistence with those of a 2D multi-layered model presented in [29] which are around 0.02 [°C·m^2/W] at frequencies above 10 GHz. As can be seen from Fig. 3, the heating factors of the models are different over the frequency range, and they are all frequency-dependent

Table 3. Comparison of maximum local SAR, SAR_{1g}, and SAR_{10g} for the forehead model with IPD of 10 W/m^2

Freq. (GHz)	Comparison of results	LocalSAR	SAR_{1g}	SAR_{10g}
77	[25]	27.2	0.58	0.27
	[22]	24.51	0.58	0.27
	Proposed here	25.37	0.58	0.27
100	[25]	33.90	0.62	0.29
	[22]	28.98	0.61	0.28
	Proposed here	29.25	0.62	0.29

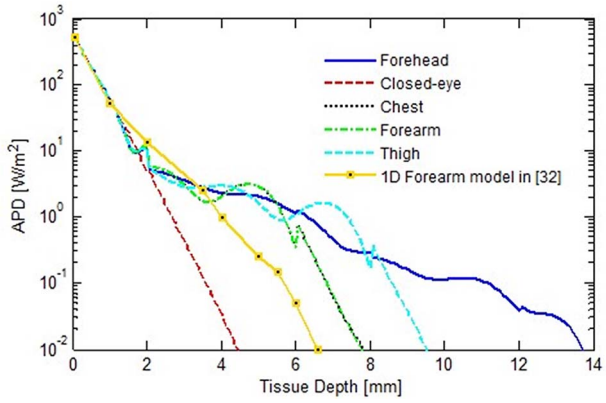

Figure 2. APDs of five different models and 1D forearm model presented in [32] when the IPD is 1000 W/m^2 for 30 GHz.

https://doi.org/10.1017/S1759078724000977 Published online by Cambridge University Press

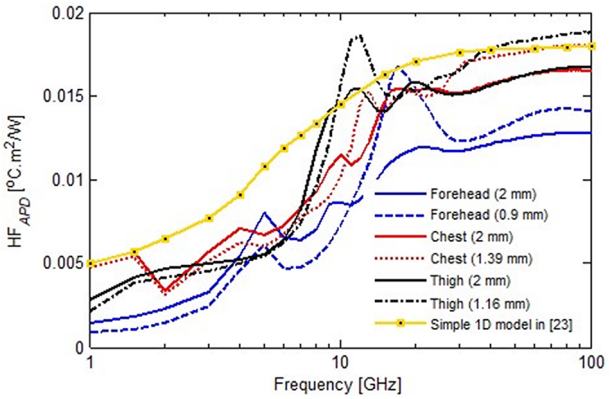

Figure 3. Heating factors of the simple 1D model in [23] and 1D models with 2 mm and realistic skin thickness.

at frequencies below 60 GHz, but not frequency-dependent at frequencies above 60 GHz. The heating factors obtained in [23] for a simple 1D model and obtained here for different 1D multi-layered models are in acceptable agreement.

Effect of skin thickness in the 1D multi-layered models on the EM exposure metrics

In Fig. 3, the heating factors of all 1D models having realistic skin thickness are compared with those having 2 mm skin thickness to show the effect of skin thickness. It can be seen from Fig. 3 that the heating factors of the models with realistic skin thickness are greater than those with 2 mm skin thickness above 30 GHz. Therefore, the heating factors of all models are significantly affected by the change in the skin thickness.

Figure 4 shows the APD distributions in the forehead, chest, and thigh models with the skin thickness of 2 mm and realistic values in Table 1 for the IPD of 1000 W/m^2 at 30 and 60 GHz. In Fig. 4, there is no significant difference in the APD distributions inside the skin tissues of the models, whereas different skin thickness of the models makes respectable difference on the APD distributions in the deeper tissues. It can be seen from Fig. 4 that APDs of the models with realistic skin thickness in the deeper tissues are higher than those of the models with 2 mm skin thickness.

PTCs of the forehead, chest, and thigh models with 2 mm and realistic skin thicknesses are shown in Fig. 5. The PTCs of different models are significantly affected by the change of skin thickness, especially at frequencies below 30 GHz. The PTC values of the models with 2 mm skin thickness are the same above 30 GHz due to their same skin thicknesses, whereas the change in the skin thickness makes a difference in the PTCs values of the models below 60 GHz. The fluctuations occurred in PTC depend on the frequency of EM exposure and the skin thickness of the models because the skin tissue of the models acts as an impedance matching layer.

EM analysis of eye layer with open and closed eyelid

Effects of the eyelid and its thickness in the eye model given in Fig. 1(b) on the EM wave exposure metrics are investigated up to 100 GHz. In the original voxel body model, the thickness of eyelid is 2 mm, whereas the realistic eyelid thickness is 0.57 mm, presented in Table 1.

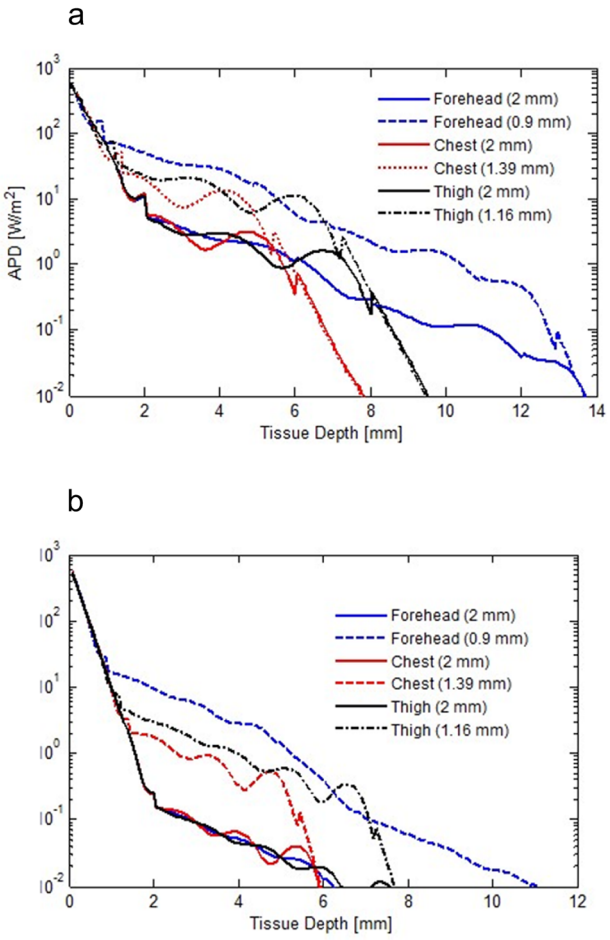

Figure 4. APDs of different models with 2 mm and realistic skin thickness for the IPD of 1000 W/m^2 at (a) 30 and (b) 60 GHz.

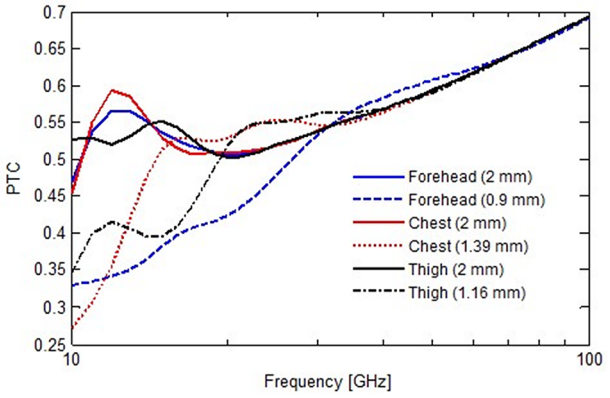

Figure 5. PTCs of the forehead, chest, and thigh 1D models with 2 mm and realistic skin thickness.

Figure 6 shows the PTCs of the open and closed eye models with 2 mm and 0.57 mm eyelid thickness. The power transmission in the eye models is significantly affected by the presence and thickness of eyelid in the eye model. Above 10 GHz, the presence of the eyelid significantly increases the power transmission, while the eyelid thickness does not make a significant difference in PTC values. It can also be noticed at frequencies between 3 GHz and 10 GHz that the power transmission in the eye model with 2 mm eyelid

https://doi.org/10.1017/S1759078724000977 Published online by Cambridge University Press

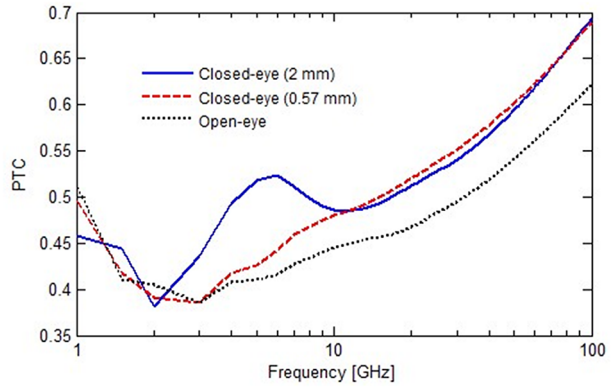

Figure 6. PTCs of the open-eye and closed-eye models with 2 mm and 0.57 mm eyelid thicknesses.

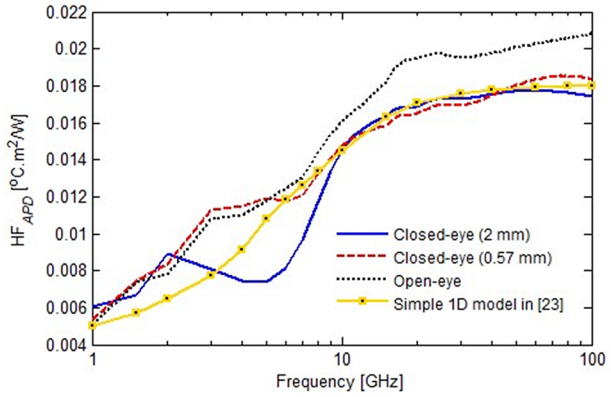

Figure 7. Heating factors of the open-eye and closed-eye models with 2 mm and realistic eyelid thicknesses.

thickness is higher than others. The heating factors of the open-eye model and closed-eye model with 2 mm and 0.57 eyelid thickness are shown in Fig. 7. The heating factors are affected by the presence and thickness of eyelid in the eye model. It is clearly seen that the heating factor values in the absence of the eyelid are higher than in the presence of the eyelid. The heating factors for all eye models are less than the recommended value of 0.025 [°C·m^2/W] in [32]. It is also worth noting that EM absorption by the eye model may also be affected by the curvature of the eye and the presence of other curved tissues on the face, such as the nose.

Conclusion

In this paper, realistic 1D multi-layered models obtained from different regions of the human body model with 2 mm skin thickness are extensively investigated using the dispersive algorithm based on the FDTD method over the frequency range from 1 to 100 GHz. Then, 1D multi-layered models with realistic skin thickness values presented in Table 1 are analyzed to show the effect of skin thickness on the EM wave exposure metrics up to 100 GHz. The calculated EM wave exposure metrics are highly affected by the tissue arrangement and skin thickness of the 1D multi-layered models. Numerical results show that the distributions of APD in the tissues of models, PTC, and heating factors of the models are really affected by the change of the skin thickness and frequency. The skin thickness and tissue arrangement of the models highly affect the PTC values at below 20 GHz, whereas they are only affected by the skin thickness at frequencies above 20 GHz. The heating factors of the models highly depend on the tissue arrangement and the skin thickness of the 1D models at frequencies up to 100 GHz. Furthermore, the effect of an eyelid and its thickness in the eye model on the EM wave exposure metrics are investigated up to 100 GHz. The presence of the eyelid makes a significant difference on the power transmission and heating factor, especially at frequencies above 10 GHz. The eyelid thickness significantly affects the heating factor and PTC at frequencies between 2 and 10 GHz, but not at frequencies above 10 GHz. The findings on the numerical results at mmWave frequency range may be useful in evaluating experiments of EM dosimetry and developing the human safety guidelines.

Funding statement. This research received no specific grant from any funding agency, commercial or not-for-profit sectors.

Competing interests. The author reports no competing interests.

References

1. **Cardis E, Deltour I, Mann S, Moissonnier M, Taki N, Varsier K and Wake J** Distribution of RF energy emitted by mobile phones in anatomical structures of the brain. *Physics in Medicine and Biology* **53**11, 2771–2783. (2008).
2. **Russell CL** 5 G wireless telecommunications expansion: Public health and environmental implications. *Environmental Research* **165**, 484–495. Aug. (2018).
3. **Dilli R** Implications of mmWave radiation on human health: State of the art threshold levels. *IEEE Access* **9**, 13009–13021. (2021).
4. **Chiaraviglio L, Elzanaty A and Alouini MS** Health risks associated with 5G exposure: A view from the communications engineering perspective. *IEEE Open Journal of the Communications Society* **2**, 2131–2179. (2021).
5. **Schuz J, Pirie K, Reeves GK, Floud S and Beral V** Cellular telephone use and the risk of brain tumors: Update of the UK million women study. *JNCI: Journal of the National Cancer Institute* **114**5, 404–711. May. (2022).
6. Study Group INTERPHONE Brain tumour risk in relation to mobile telephone use: Results of the INTERPHONE international case-control study. *International Journal of Epidemiology* **41**1, 675–694. Feb. 2012.
7. International Commission on Non-Ionizing Radiation Protection Guidelines for limiting exposure to electromagnetic fields (100 kHz to 300 GHz). *Health Physics* **118**(5), 483–524. (2020).
8. IEEE standard for safety levels with respect to human exposure to electric, magnetic and electromagnetic fields, 0 Hz to 300 GHz, Standard C95.1-2019, 2019.
9. **Kodera S, Taguchi K, Diao Y, Kashiwa T and Hirata A** Computation of whole-body average SAR in realistic human models from 1 to 100 GHz. *IEEE Transactions on Microwave Theory and Techniques* **72**1, 91–100. Jan. (2024).
10. **Wang J and Fujiwara O** FDTD computation of temperature rise in the human head for portable telephones. *IEEE Transactions on Microwave Theory and Techniques* **47**, 1528–1534. Aug. (1999).
11. **Bernardi P, Cavagnaro M, Pisa S and Piuzzi E** Specific absorption rate and temperature increases in the head of a cellular-phone user. *IEEE Transactions on Microwave Theory and Techniques* **48**7, 1118–1126. July. (2000).
12. **Hirata A, Matsuyama S and Shiozawa T** Temperature rises in the human eye exposed to EM waves in the frequency range 0.6-6 GHz. *IEEE Transactions on Electromagnetic Compatibility* **42**4, 386–393. Nov. (2000).
13. **Hirata A, Morita M and Shiozawa T** Temperature increase in the human head due to a dipole antenna at microwave frequencies. *IEEE Transactions on Electromagnetic Compatibility* **45**1, 109–116. Feb. 2003.
14. **Hirata A and Fujiwara O** The correlation between mass-averaged SAR and temperature elevation in the human head model exposed to RF near-fields

from 1 to 6 GHz. *Physics in Medicine and Biology* **54**23, 7227–7238. Dec. (2009).
15. **Wessapan T and Rattanadecho P** Specific absorption rate and temperature increase in the human eye due to electromagnetic fields exposure at different frequencies. *International Journal of Heat and Mass Transfer* **64**, 426–435. 2013.
16. **Hirata A, Laakso I, Oizumi T, Hanatani R, Chan KH and Wiart J** The relationship between specific absorption rate and temperature elevation in anatomically based human body models for plane wave exposure from 30 MHz to 6 GHz. *Physics in Medicine and Biology* **58**4, 903–921. (2013).
17. **Kaburcuk F and Elsherbeni AZ** Temperature rise and SAR distribution at wide range of frequencies in a human head due to an antenna radiation. *ACES Journal* **33**4, 367–372. April. (2018).
18. **Kaburcuk F and Elsherbeni AZ** Efficient computation of SAR and temperature rise distributions in a human head at wide range of frequencies due to 5G RF field exposure. *ACES Journal* **33**11, 1236–1242. Nov. (2018).
19. **Kuster N, Santomaa V and Drossos A** The dependence of electromagnetic energy absorption upon human head tissue composition in the frequency range of 300-3000 MHz. *IEEE Transactions on Microwave Theory and Techniques* **48**11, 1988–1995. (2000).
20. **Samaras T, Christ A and Klingenbock A** Worst case temperature rise in a one-dimensional tissue model exposed to radiofrequency radiation. *IEEE Transactions on Biomedical Engineering* **54**3, 492–496. Mar. (2007).
21. **Sabbah AI, Dib NI and Al-Nimr MA** Evaluation of specific absorption rate and temperature elevation in a multi-layered human head model exposed to radio frequency radiation using the finite-difference time domain method. *IET Microwaves, Antennas & Propagation* **5**9, 1073–1080. (2011).
22. **Kaburcuk F, Elsherbeni AZ, Lumnitzer R and Tanner A** Electromagnetic waves interaction with a human head model for frequencies up to 100 GHz. *ACES Journal* **35**6, 613–621. Jun. 2020.
23. **Funahashi D, Hirata A, Kodera S and Foster KR** Area-averaged transmitted power density at skin surface as metric to estimate surface temperature elevation. *IEEE Access* **6**, 77665–77674. (2018).
24. **Laakso I, Morimoto R, Heinonen J, Jokela K and Hirata A** Human exposure to pulsed fields in the frequency range from 6 to 100 GHz. *Physics in Medicine & Biology* **62**17, 6980–6992. 2017.
25. **Gustrau F and Bahr A** W-band investigation of material parameters, SAR distribution, and thermal response in human tissue. *IEEE Transactions on Microwave Theory and Techniques* **50**10, 2393–2400. Oct. 2002.
26. **Laakso I** Assessment of the computational uncertainty of temperature rise and SAR in the eyes and brain under far-field exposure from 1 to 10 GHz. *Physics in Medicine and Biology* **54**, 3393–3404. 2009. 10.1088/0031-9155/54/11/008.
27. **Morimoto R, Laakso I, De Santis V and Hirata A** Relationship between peak spatial-averaged specific absorption rate and peak temperature elevation in human head in frequency range of 1–30 GHz. *Physics in Medicine and Biology* **61**, 5406–5425. (2016).
28. **Morimoto R, Hirata A, Laakso I, Ziskin MC and Foster KR** Time constants for temperature elevation in human models exposed to dipole antennas and beams in the frequency range from 1 to 30 GHz. *Physics in Medicine and Biology* **62**, 1676–1699. 2017. 10.1088/1361-6560/aa5251.
29. **Diao Y, Rashed EA and Hirata A** Assessment of absorbed power density and temperature rise for nonplanar body model under electromagnetic exposure above 6 GHz. *Physics in Medicine & Biology* **65**22, Nov. (2020). 224001.
30. **Elsherbeni AZ, and Demir V** *The Finite-Difference Time-Domain Method for Electromagnetics With MATLAB Simulations*, 2nd ed. Edison, NJ, USA: SciTech, 2016.
31. **Hashimoto Y, Hirata A, Morimoto R, Aonuma S, Laakso I, Jokela K and Foster KR** On the averaging area for incident power density for human exposure limits at frequencies over 6 GHz. *Physics in Medicine and Biology* **62**8, 3124–3138. Mar. 2017.
32. **Sasaki K, Mizuno M, Wake K and Watanabe S** Monte Carlo simulations of skin exposure to electromagnetic field from 10 GHz to 1 THz. *Physics in Medicine & Biology* **62**17, 6993–7010. (2017).
33. **Y. L and K. H** Skin thickness of Korean adults. *Surgical and Radiologic Anatomy* **24**, 183–189. (2002).
34. **Nagaoka T, Watanabe S, Sakurai K, Kunieda E, Watanabe S, Taki M and Yamanaka Y** Development of realistic high-resolution whole-body voxel models of Japanese adult males and females of average height and weight, and application of models to radio-frequency electromagnetic-field dosimetry. *Physics in Medicine and Biology* **49**1, 1–15. Jan. (2004).
35. **Diao Y, Leung S-W, He Y, Sun W, Chan K-H, Siu Y-M et al.** Detailed modeling of palpebral fissure and its influence on SAR and temperature rise in human eye under GHz exposures. *Bioelectromagnetics* **37**4, 256–263. May. (2016).
36. **Bernardi P, Cavagnaro M and Pisa S** Assessment of the potential risk for humans exposed to millimeter-wave wireless LANs: The power absorbed in the eye. *Wireless Networks* **3**, 511–517. (1997).
37. **Lumnitzer RS**, Energy Harvesting Near the Human Body Using Finite-Difference Time-Domain Simulations. Diss. Colorado School of Mines, (2023).
38. **Li K and Sasaki K** Monte Carlo simulation of clothed skin exposure to electromagnetic field with oblique incidence angles at 60 GHz. *Frontiers in Public Health* **10**(795414),(2022)
39. **Li K, Hikage T, Masuda H, Ijima E, Nagai A and Taguchi K** Parameter variation effects on millimeter wave dosimetry based on precise skin thickness in real rats. *Scientific Reports* **13**1, Oct. (2023). 17397.
40. **Pennes HH** Analysis of tissue and arterial blood temperatures in the resting human forearm. *Journal of Applied Physiology* **1**, 93–122. (1948).
41. **Hirata A, Fujiwara O and Shiozawa T** Correlation between peak spatial-average SAR and temperature increase due to antennas attached to human trunk. *IEEE Transactions on Biomedical Engineering* **53**8, 1658–1664. (2006).

Fatih Kaburcuk received both the M.Sc. and Ph.D. degrees from Syracuse University, Syracuse, NY, USA, in 2011 and 2014, respectively, all in electrical engineering. During his graduate studies, he worked as a Research Assistant with Syracuse University and PPC-Belden Inc. in Liverpool, NY, USA. He worked as a Visiting Research Scholar at the Department of Electrical Engineering, Colorado School of Mines, Golden, CO, USA in 2014. He joined the Erzurum Technical University and Sivas Cumhuriyet University in 2015 and 2019, respectively. Dr. Kaburcuk is currently an Associate Professor in the Department of Electrical-Electronics Engineering at Sivas University of Science and Technology, Sivas, Turkey. Dr. Kaburcuk is the Associated Editor for Applied Computational Electromagnetics Society (ACES) Journal. His research interests include numerical methods in electromagnetics, biological effect of electromagnetic radiation, and finite-difference time-domain analysis of antennas and RF devices.

https://doi.org/10.1017/S1759078724000977 Published online by Cambridge University Press